Symmetry breaking of Gamow-Teller and magnetic-dipole transitions and its restoration in calcium isotopes

Tomohiro Oishi [1,2,*] Ante Ravlić [2,†] and Nils Paar[2,‡]

[1]*Yukawa Institute for Theoretical Physics, Kyoto University, Kyoto 606-8502, Japan*
[2]*Department of Physics, Faculty of Science, University of Zagreb, Bijenička cesta 32, HR-10000 Zagreb, Croatia*

Nuclear magnetic-dipole ($M1$) and Gamow-Teller (GT) transitions provide insight into the spin-isospin properties of atomic nuclei. By considering them as unified spin-isospin transitions, the $M1$/GT transition strengths and excitation energies are subject to isospin symmetry. The excitation properties associated to the $M1$/GT symmetry need to be clarified within a consistent theoretical approach. In this work, the relationship between the $M1$ and GT transitions in Ca isotopes is investigated in a unified framework based on the relativistic energy-density functional (REDF) with point-coupling interactions, using the relativistic quasiparticle random-phase approximation (RQRPA). It is shown that the isovector-pseudovector (IV-PV) residual interaction affects both transitions, and the symmetry of $M1$ and giant-GT transitions is disrupted by this interaction in closed-shell nuclei. In open-shell Ca isotopes, the proton-neutron pairing in the residual RQRPA interaction also plays a role in GT transitions. Due to the interplay between these interactions, the $M1$/GT symmetry can be restored especially in the ^{42}Ca nucleus, i.e., the giant-GT strength can become comparable to that of the $M1$ mode in terms of the unified spin-isospin transitions by adjusting the proton-neutron pairing strength to reproduce the experimental low-lying GT-excitation energies. The mirror symmetry of both $M1$ and GT transitions is also demonstrated for open-shell mirror partners, ^{42}Ca and ^{42}Ti. Further improvements are required to achieve simultaneous reproduction of $M1$ and GT transition energies in the REDF framework.

I. INTRODUCTION

Nuclear magnetic-dipole ($M1$) and Gamow-Teller (GT) modes have attracted interest in their isospin symmetry [1,2]. The GT operator for an A-nucleon system formally reads $\sum_{k \in A} \hat{\tau}_{\pm}(k)\hat{\boldsymbol{\sigma}}(k)$, where $\hat{\tau}$ and $\hat{\sigma}$ indicate the isospin and spin, respectively. For the spin-flip $M1$ transition, on the other side, its isovector (IV) operator is given as $\sum_{k \in A} \hat{\tau}_0(k)\hat{\boldsymbol{\sigma}}(k)$ by neglecting physical factors. Therefore, the GT and IV-spin $M1$ transitions can be interpreted as the unified spin-isospin transition, and a similarity based on the isospin symmetry is expected. Theoretically, both the GT and $M1$ transitions are roughly understood by considering the spin-orbit (SO) splitting and relevant residual interactions [3–5] (see also Refs. [6–12] for $M1$ and and Refs. [13–17] for GT transitions). In open-shell nuclei, the isoscalar and isovector pairing correlations have been shown as relevant [12,14,18–24].

The GT transition is one of the main ingredients of β radioactivity [25–27]. It plays an essential role in nucleosynthesis especially by determining the β-decay lifetimes, which provide a key ingredient for understanding the r-process timescale [26–28]. Furthermore, evaluation of the GT strength is important in order to predict the neutrino-induced reactions

and electron capture in nuclei during the late stages of stellar evolution [29,30]. In Refs. [17,19], the GT resonances are reproduced by improving the spin-isospin parameters in the Skyrme energy-density functional (EDF). Recently in Ref. [31], by utilizing the subtracted second Skyrme random-phase approximation (RPA), the GT strengths of ^{48}Ca and ^{78}Ni are obtained in better agreement with experiments than the other EDF calculations. In addition, one remarkable advantage in studies on GT modes is the existence of the Ikeda-Fujii-Fujita sum rule [32,33]. This rule has provided an essential constraint to validate studies of GT resonances and spin-isospin properties in nuclei [13–19,31,34–36].

The $M1$ transition is the leading mode of magnetic transitions [25,37–40], and has been theoretically studied by utilizing the nonrelativistic RPA [6–10,41–43], relativistic RPA [11,12], shell-model calculations [44–47], etc. For further information, see the references in reviews [37,38]. In Refs. [45,46], the analogy with neutrino-nucleus scattering is discussed. It also plays a role in the determination of neutron-capture rates, of significance for the r-process nucleosynthesis [46,48,49]. In Ref. [47], the minor (finite) quenching of the IS (IV) $M1$ strength is concluded. There exists Kurath's sum rule for the $M1$ transitions in the case where the single-orbit approximation is applicable [50]. In the nonrelativistic RPA studies [6–10], the RPA-residual interaction essentially contributes in determining the $M1$ energy and strength, and its importance is also concluded in the relativistic RPA studies [11,12].

———————
*tomohiro.oishi@yukawa.kyoto-u.ac.jp
†aravlic@phy.hr
‡npaar@phy.hr

For experimental measurement of GT transitions, two procedures have been utilized, namely, those from β radioactivity and charge-exchange (CE) reactions. The β radioactivity may provide direct information on the GT strength B_{GT} [25,26]. However, its experimental accessibility is limited by the energy release (Q value). The CE reactions by strong-interaction probes, on the other side, enable one to measure the GT transitions toward higher energies. The famous examples include the CE excitations by the (p, n) as well as $(^3\mathrm{He}, t)$ reactions [27,51–55]. For $M1$ transitions, although its concept originates in the electromagnetic interaction, those can be measured also with the common strong-interaction probes [27,47,56–58]. Namely, assuming the isospin symmetry, this type of $M1$ transition can be interpreted as the isobaric-analog component in the same category of GT transitions. Recent developments of experiments provide a rich amount of data to this aim. However, the expected symmetry between these $M1$ and GT transitions has not been completely validated. In addition, for improvement of theoretical models, the simultaneous reproduction of these $M1$/GT properties could be used as a standard benchmark.

In this work, we discuss the $M1$ and GT transitions within a common framework of the relativistic energy-density functional (REDF) theory [36,59–65]. By utilizing the relativistic quasiparticle random-phase approximation (RQRPA) [14,66,67], we discuss the relationship between $M1$ and GT transitions. The validity of current REDF parametrization is examined from the experimental $M1$ and GT data.

In this paper, we use the CGS-Gauss system of units. Also, all the systems discussed in the following sections are assumed as spherical.

II. FORMALISM

The relativistic mean-field calculation and RQRPA developed in Refs. [11,12,36,64,68] are utilized in this work. We briefly review the formalism and setting of parameters. Our calculation is based on the point-coupling REDF determined from the Lagrangian density,

$$\mathcal{L} = \mathcal{L}_{\mathrm{PC}} + \mathcal{L}_{\mathrm{IV\text{-}PV}}, \tag{1}$$

where $\mathcal{L}_{\mathrm{PC}}$ includes the isoscalar-scalar, isoscalar-vector, and isovector-vector coupling terms with point-coupling (PC) interaction [68,69]. In this work, two parametrizations of density-dependent PC interactions are used, DD-PC1 [69] and DD-PCX [70]. In addition, for description of GT and $M1$ transitions, the isovector-pseudovector (IV-PV) Lagrangian density is included, where it contributes to the RQRPA residual interaction [62,67,71]. That is,

$$\mathcal{L}_{\mathrm{IV\text{-}PV}} = -\hbar c \frac{\alpha_{\mathrm{IV\text{-}PV}}}{2} [\bar{\psi} \gamma_5 \gamma_\mu \vec{\tau} \psi][\bar{\psi} \gamma_5 \gamma^\mu \vec{\tau} \psi]. \tag{2}$$

Note that, since this IV-PV term leads to the parity-violating mean field at the Hartree level, it does not contribute to the solution of natural-parity states, including the 0^+ ground state. In the nonrelativistic limit, the IV-PV interaction derived from this Lagrangian density corresponds to the spin-isospin term in the Landau-Migdal interaction [12].

TABLE I. Interactions used in our RHB and RQRPA calculations. The label ph (pp) indicates the quasiparticle-quasihole (quasiparticle-quasiparticle) channel.

		$M1$	GT
RHB (0^+)	ph	DD-PC1/DD-PCX	
	pp	T1 pairing	
RQRPA (1^+)	ph	DD-PC1/DD-PCX plus IV-PV	
	pp	T1 pairing	PN (T0) pairing

For open-shell nuclei, pairing correlations in the particle-particle (pp) channel should be taken into account. For this purpose, we employ the same model used in Refs. [11,62,68,69]. Namely, for isospin-triplet (T1) pairs of proton-proton and neutron-neutron, a finite-range two-Gaussian potential is used. That is,

$$V_{\mathrm{pp,T1}}(d) = \sum_{i=1,2} e^{-d^2/\mu_i^2} \big(W_i + B_i \hat{P}^\sigma \\ - H_i \hat{P}^\tau - M_i \hat{P}^\sigma \hat{P}^\tau \big), \tag{3}$$

where $d = |\mathbf{r}_2 - \mathbf{r}_1|$. The operators $\hat{P}^\sigma$ and $\hat{P}^\tau$ indicate the exchanges of the spin and isospin, respectively. Its parameters μ_i, W_i, B_i, H_i, and M_i are taken from the central part of the Gogny-D1S force in Ref. [72]. Therefore, both in the $M1$ and GT cases, the ground state is obtained from the relativistic Hartree-Bogoliubov (RHB) method with the DD-PC1 and T1-pairing parameters in the particle-hole and particle-particle channels, respectively. This T1 pairing is also used in the RQRPA for $M1$ transitions.

For isospin-singlet (T0) proton-neutron (PN) pairing, on the other side, we assume the same potential used in the PN-RQRPA calculations in Refs. [14,73,74], i.e., the similar two-Gaussian potential but only active in the $S_{12} = 1$ channel. That is,

$$V_{\mathrm{pp,T0}}(d) = f \left[-G_0 \sum_{i=1,2} e^{-d^2/v_i^2} g_i \right] \Pi_{S_{12}=1, T_{12}=0}, \tag{4}$$

where $\Pi_{S_{12}=1, T_{12}=0}$ indicates the projection into the ($S_{12} = 1, T_{12} = 0$) channel. Here parameters G_0, g_i, and v_i are the same as utilized in Ref. [74] but with the strength parameter $f = 0.81$ adjusted to reproduce the low-lying GT($-$) excitation energy of $^{42}\mathrm{Ca}$, 0.611 MeV [75], which is shown in Sec. III C. We have summarized the interactions used for the ground-state (RHB) as well as the excited-state (RQRPA) calculations in Table I.

We use the isospin convention as $\hat{\tau}_0(k) |k\rangle = \tau_0 |k\rangle$ with $\tau_0 = 1 (-1)$ when the kth nucleon is a neutron (proton). The GT operator thus reads

$$\hat{\mathcal{O}}_\nu^{\mathrm{GT}(\pm)} = \sum_{k \in A} \hat{\tau}_\pm(k) \hat{s}_\nu(k), \tag{5}$$

where $\nu = \pm 1$ or 0 (magnetic quantum number). The isospin operator $\hat{\tau}_\pm(k)$ changes the charge of the kth nucleon in the GT($\pm$) transition. Notice that the spin operator $\hat{s}_\nu$ is used instead of $\hat{\sigma}_\nu = 2\hat{s}_\nu$, and thus, the present definition is different by a factor of $1/2$ from the usual GT operator. On the other

side, the IV $M1$ operator reads

$$\hat{\mathcal{O}}_\nu^{M1} = \mu_N \sqrt{\frac{3}{4\pi}} \sum_{k \in A} \hat{\tau}_0(k)[g_s \hat{s}_\nu(k) + g_l \hat{l}_\nu(k)], \quad (6)$$

where μ_N indicates the nuclear magneton, and the nuclear g factors for the IV $M1$ mode are $g_s = 4.706$ and $g_l = 1/2$ [50,76]. However, with respect to the GT operator, we neglect the orbital-$M1$ component, $\hat{\tau}_0 \hat{l}_\nu$, except when mentioned. We also omit the factors g_s and $\mu_N \sqrt{3/4\pi}$ in the following sections. This omission corresponds to the renormalization of B_{M1} as in Ref. [77]. Namely, we employ the IV spin-$M1$ operator,

$$\hat{\mathcal{O}}_\nu^{M1S} = \sum_{k \in A} \hat{\tau}_0(k)\hat{s}_\nu(k), \quad (7)$$

which is in correspondence to the GT operator. In this work the so-called quenching factors on $M1$ and GT operators are not considered, for simplicity.

For the orbital-$M1$ component, $\hat{\tau}_0 \hat{l}_\nu$, its contribution to the IV $M1$ response is indeed finite, but it does not change the $M1$ excitation energies. We describe its details in the Appendix. In the main text, we neglect this "inclusion" into the unified spin-isospin modes, and consider their operators as in Eqs. (5) and (7).

The charge-conserving RQRPA is utilized for the IV-spin-$M1$ mode. Using the quasiparticle random phase approximation (QRPA) ansatz, the $M1$-excited state $|\omega\rangle$ is formally given as

$$\hat{\mathcal{H}} |\omega\rangle = \hbar\omega |\omega\rangle, \quad |\omega\rangle = \hat{\mathcal{Z}}_{M1}^\dagger(\omega) |\Phi\rangle, \quad (8)$$

where $|\Phi\rangle$ is the RHB ground state and $\hbar\omega$ is the excitation energy. The $M1$-excitation operator reads

$$\hat{\mathcal{Z}}_{M1}^\dagger(\omega) = \sum_{\rho < \sigma} \{X_{\rho\sigma}(\omega)\hat{\mathcal{Q}}_{\sigma\rho}^\dagger - Y_{\rho\sigma}^*(\omega)\hat{\mathcal{Q}}_{\sigma\rho}\}, \quad (9)$$

with $\hat{\mathcal{Q}}_{\sigma\rho} = [\hat{a}_\sigma \otimes \hat{a}_\rho]^{(J,P)}$ coupled to the $J^P = 1^+$ spin and parity. Here $\hat{a}_\sigma$ is the quasiparticle operator with the label σ for quantum numbers. The labels (ρ, σ) indicate proton-proton and neutron-neutron pairs. In the PN-RQRPA for GT($\pm$) modes [14,67], on the other side, it reads

$$\hat{\mathcal{Z}}_{GT}^\dagger(\omega) = \sum_{\alpha,\beta} \{X_{\alpha\beta}(\omega)\hat{\mathcal{Q}}_{\beta\alpha}^\dagger - Y_{\alpha\beta}^*(\omega)\hat{\mathcal{Q}}_{\beta\alpha}\}, \quad (10)$$

where labels (α, β) indicate proton-neutron 1^+ pairs. Then, by solving the matrix form of the QRPA equation, excitation amplitudes are obtained:

$$\begin{pmatrix} A & B \\ B^* & A^* \end{pmatrix} \begin{pmatrix} X(\omega) \\ Y^*(\omega) \end{pmatrix} = \hbar\omega \begin{pmatrix} I & 0 \\ 0 & -I \end{pmatrix} \begin{pmatrix} X(\omega) \\ Y^*(\omega) \end{pmatrix}, \quad (11)$$

where A and B are the well-known QRPA matrices [66,67,78]. From the RQRPA solutions $|\omega_f\rangle$ with $E_f = \hbar\omega_f$, response functions can be obtained as

$$R_X(E) = \sum_f \delta(E - E_f)B_X(E_f)$$
$$= \sum_f \delta(E - E_f) \sum_{\nu = \pm 1, 0} \left| \langle f | \hat{\mathcal{O}}_\nu^X | \Phi \rangle \right|^2, \quad (12)$$
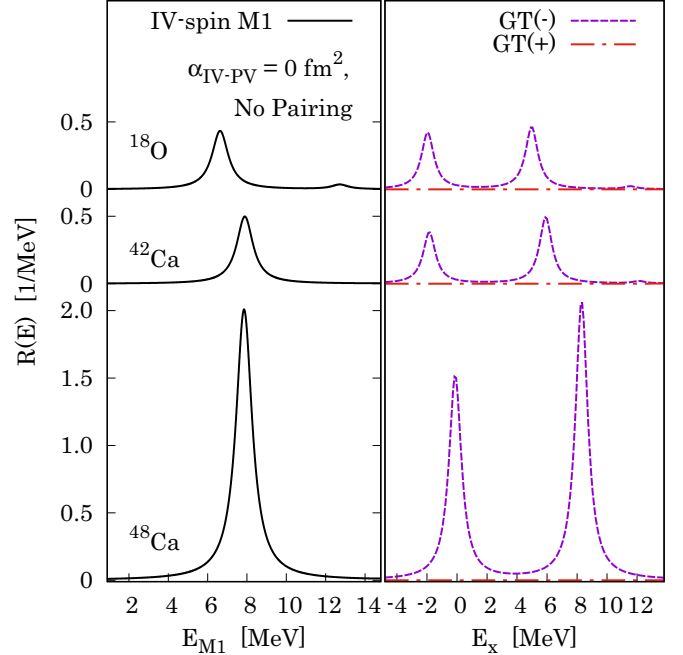

FIG. 1. The nonperturbed IV-spin-$M1$ and GT($\pm$) strength distributions obtained with the DD-PC1 interaction. The GT($\pm$)-excitation energies E_x are presented with respect to the daughter nuclei [73].

for $X = M1S$ and GT($\pm$). For the purpose of visualization, these response functions are smeared with the normalized Cauchy-Lorentz profile, whose full width at half maximum (FWHM) is 1.0 MeV in this work. For magic nuclei, corresponding to the zero-pairing limit, the RQRPA reduces to the relativistic random-phase approximation (RRPA). Similarly to Refs. [11,12], our RHB and R(Q)RPA calculations are performed in the model space expanded in the harmonic oscillator (HO) basis up to 20 major shells. The cutoff energy of 120 MeV for the configuration space in the QRPA is checked to be sufficient to have the convergence of results.

III. RESULTS

A. Nonperturbed response

Before going to the full consideration of the RQRPA calculations, first we show the nonperturbed responses for the GT and $M1$ transition operators. They are obtained by neglecting the residual RQRPA interaction, thus keeping only the response calculated with the DD-PC1 interaction. The pairing (pp) correlations in the ground states are also neglected.

In Fig. 1, the nonperturbed response functions for GT and $M1$ modes obtained with the DD-PC1 interaction are displayed for ^{18}O, ^{42}Ca, and ^{48}Ca. Since their operators introduced in Eq. (5) have the identical form of $\hat{\tau}\hat{s}$, their responses can be directly compared. Note that, for GT($\pm$) modes, their excitation energies are given with respect to the ground states of daughter nuclei by using the converting method in Ref. [73].

First we focus on the isobaric-analog symmetry between the IV-spin-$M1$ and the giant, higher-energy GT($-$)

transitions. For all three nuclei shown in Fig. 1, the non-perturbed IV-spin-$M1$ strength is equal to the higher-energy GT($-$) strength: $R_{M1} \cong R_{GT(-)}(E_x)$ with $E_x = 5.4$, 6.6, and 8.5 MeV in ^{18}O, ^{42}Ca, and ^{48}Ca, respectively. By analyzing the transition components, this equivalence can be explained from the identical set of quasiparticle transitions. That is,

$$\nu(1d_{5/2}) \longrightarrow \nu(1d_{3/2}) \text{ in IV } M1 \text{ and}$$

$$\nu(1d_{5/2}) \longrightarrow \pi(1d_{3/2}) \text{ in GT}(-),$$

for ^{18}O, where the symbol π (ν) indicates the proton (neutron) state. Similarly for ^{42,48}Ca,

$$\nu(1f_{7/2}) \longrightarrow \nu(1f_{5/2}) \text{ in IV } M1 \text{ and}$$

$$\nu(1f_{7/2}) \longrightarrow \pi(1f_{5/2}) \text{ in GT}(-).$$

Because the form of operators and the set of quantum labels are identical, it is natural to produce the same amount of transition strength in these two modes.

On the GT($-$) side in Fig. 1, there is another, low-lying peak. This low-lying GT response is attributable to the charge-exchange transition of $\nu(j = l + 1/2) \to \pi(j = l + 1/2)$ [14]. That is, for ^{18}O,

$$\nu(1d_{5/2}) \longrightarrow \pi(1d_{5/2}) \text{ in GT}(-),$$

whereas, for ^{42,48}Ca,

$$\nu(1f_{7/2}) \longrightarrow \pi(1f_{7/2}) \text{ in GT}(-).$$

Notice that its isobaric-analog transition of $M1$ type is non-physical because the initial and final states are in this case identical.

In Fig. 1 the nonperturbed low-lying GT($-$) responses show the negative excitation energies. This implies that, by neglecting the residual RQRPA interactions, the calculated GT($-$) energies of daughter nuclei inevitably result lower than the experimental ground-state energies. This drawback is remedied in the next section by including the residual interactions.

By comparing the nonperturbed $M1$ and GT($-$) energies in Fig. 1, one can observe that $E_{M1} \cong \Delta E_{GT(-)}$ for each nucleus, where $\Delta E_{GT(-)}$ is the gap between the higher and lower GT($-$) energies. This is trivial because E_{M1} ($\Delta E_{GT(-)}$) corresponds to the SO-splitting gap of relevant orbits of neutrons (protons). Since the relevant SO splitting is of the same lj numbers, the E_{M1} and $\Delta E_{GT(-)}$ values are also similar.

For these nuclei, the GT($+$), as well as proton-$M1$ transitions, are strongly suppressed by the Pauli blocking effect. By comparing the results for Ca isotopes, one can read that the nonperturbed $M1$ and GT responses are proportional to the number of valence neutrons around the ^{40}Ca core, namely, $B_X(^{48}\text{Ca}) \cong 4B_X(^{42}\text{Ca})$ both for $X = M1$ and GT. This is simply because the ^{40}Ca nucleus cannot be active for either $M1$ or GT transitions.

Note that, for the ^{18}O and ^{42}Ca nuclei, the two-valence-nucleon $M1$ sum rule [20] was consistently reproduced in the nonperturbed relativistic RPA [11]. For the ^{42}Ca and ^{48}Ca nuclei, in addition, Kurath's $M1$ sum rule [50] was also reproduced: its details were presented in Ref. [12]. On the GT side, the Ikeda-Fujii-Fujita sum rule [32,33] can be reproduced
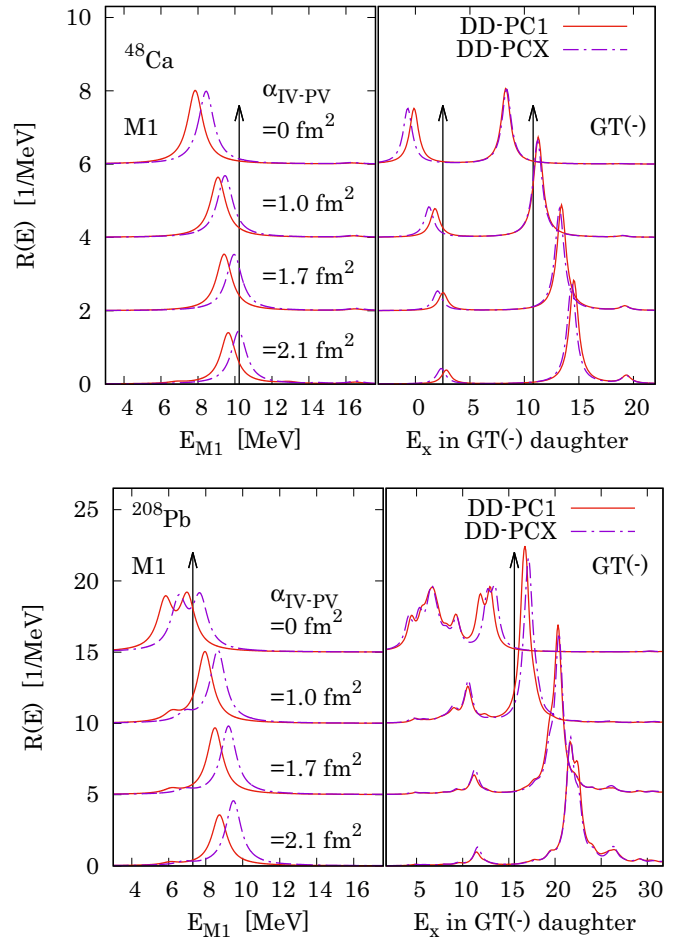

FIG. 2. Top: The IV-spin-$M1$ and GT($-$) strength distributions for ^{48}Ca with the DD-PC1 and DD-PCX interactions supplemented with the IV-PV residual interaction in the RRPA. The arrows indicate the experimental $M1$ and GT($-$) energies: $E_{M1} = 10.23$ MeV [79]; $E_{GT} = 2.517$ MeV [75] and $\cong 10.8$ MeV [80]. Several values for the IV-PV coupling constant are used, i.e., $\alpha_{IV\text{-}PV} = 0$, 1.0, 1.7, and 2.1 fm^2. For the GT($-$) mode, the excitation energy is presented with respect to the ground state of the daughter ^{48}Sc nucleus. Bottom: The same plot but for ^{208}Pb. The experimental $M1$ and GT($-$) energies are measured as $E_{M1} \cong 7.3$ MeV [81] and $E_{GT} = 15.6$ MeV [82,83].

up to 90–95% with a small deficiency due to omitting the Dirac-sea states at the R(Q)RPA level [14,66,67].

B. IV-PV residual interaction

Next we employ the IV-PV Lagrangian density $\mathcal{L}_{IV\text{-}PV}$, which contributes at the level of the R(Q)RPA residual interaction [62,67,71]. In Fig. 2, the $M1$ and GT distributions are presented for ^{48}Ca and ^{208}Pb, by using the DD-PC1 and DD-PCX interactions combined with the IV-PV interaction term with the coupling constant, $\alpha_{IV\text{-}PV}$. Notice that the pairing correlations vanish in these closed-shell systems.

As a general result in both GT($-$) and $M1$ cases in Fig. 2, the IV-PV interaction works as an additional repulsion, which increases the 1^+-excitation energies. Namely, the single-particle energies and their SO-splitting gaps depend

on the spin-parity value of the total system, J^P, because the IV-PV interaction becomes active (inactive) for the 1^+ (0^+) states [62,67,71].

For the GT(−) transition of ^{48}Ca $\longrightarrow$ ^{48}Sc, the recent experiment by Fujita *et al.* reports the first major peak at $E_{GT} = 2.517$ MeV in the daughter ^{48}Sc nucleus as the low-lying GT excitation [75], whereas the second, giant GT resonance is found around 9–14 MeV with wide fragmentation [75,80]. Compared with this set of experimental data, our calculation becomes consistent when the IV-PV coupling, $\alpha_{IV-PV} = 1.70$ fm^2, is used with the DD-PC1 interaction: the RRPA results in $E_x = 2.53$ and 13.43 MeV for the two GT(−) peaks. Note that the second GT(−) peak is expected as the transition to the continuum above the proton-separation threshold, 9.45 MeV, in ^{48}Sc [84]. Therefore, as measured in Refs. [75,80], its width can be more fragmented than our smearing assumption. For elucidating this fragmentation, one may need to employ, e.g., the continuum effects [85,86] and/or the higher-order configurations [3,31,34,53,87,88], which go beyond the present RQRPA approach. On the other side, with respect to the experimental $M1$ excitation energy, $E_{M1} = 10.23$ MeV in ^{48}Ca [79], the present setting of $\alpha_{IV-PV} = 1.70$ fm^2 is a good approximation; i.e., the RRPA with DD-PC1 gives the $M1$ excitation energy of 9.42 MeV. Considering the general accuracy of the IV-PV parameter, however, we should mention that the simultaneous reproduction of $M1$ and GT energies for various nuclei is still demanding. To further exemplify this point, the results for GT and $M1$ strength functions for ^{208}Pb are presented in the lower panel of Fig. 2. One can observe that the current setting of $\alpha_{IV-PV} = 1.70$ fm^2 with DD-PC1 overshoots its $M1$ and GT(−) energies by 1–2 MeV.

A similar problem occurs when we employ the DD-PCX interaction [70] as shown in Fig. 2. For the ^{48}Ca nucleus, by using $\alpha_{IV-PV} = 2.1$ fm^2 for the IV-PV coupling, the experimental $M1$ and low-lying GT energies are well reproduced. Simultaneously, however, this result overshoots the experimental energy of giant GT resonance, $E_{GT} \cong 10.8$ MeV in ^{48}Sc [80]. Also, for ^{208}Pb as another example, the present setting does not match with the experimental $M1$ and GT energies [81,83]. Consequently, the simultaneous reproduction of $M1$ and GT energies for light and heavy systems is challenging in the present context of DD-PCX plus IV-PV interaction. For quantitative agreement, one may need, e.g., the system-dependent tuning of $\alpha_{IV-PV} \longrightarrow \alpha_{IV-PV}(N, Z)$ and/or more complicated parametrization of the IV-PV Lagrangian. These tasks go beyond our present scope. Note also that the present IV-PV coupling constant adjusted to the GT energy in ^{48}Ca is larger than that in our previous works [11,12]. This is because, in Refs. [11,12], the parameter was adjusted differently, i.e., to the mean value of $M1$ energies of ^{48}Ca and ^{208}Pb nuclei.

Figure 2 describes how the IV-PV interaction disrupts the equivalence of strength between the $M1$ and the giant, higher-energy GT(−) transitions. Remember that, in the nonperturbed case with $\alpha_{IV-PV} = 0$, these two peaks can be attributed to the transition between $(1f_{7/2})$ and $(1f_{5/2})$ states to yield the equivalent $B_{M1/GT}$ values. Then, with $\alpha_{IV-PV} \neq 0$, the
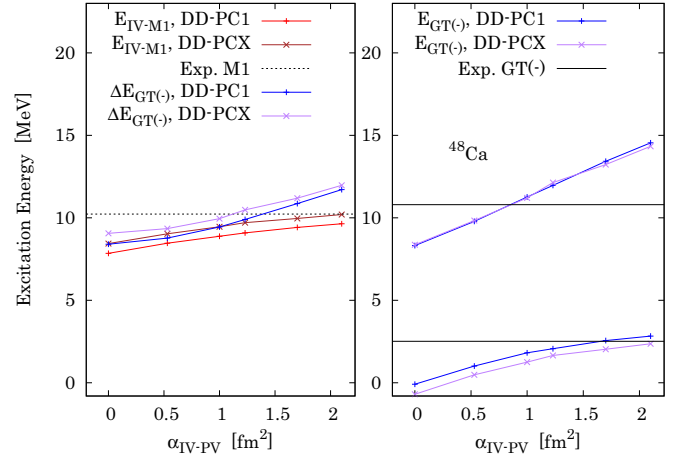

FIG. 3. The $M1$ and GT(−) excitation energies for ^{48}Ca obtained with the DD-PC1 and DD-PCX interactions supplemented with the IV-PV residual interaction for the range of values of its coupling constant α_{IV-PV}. The $\Delta E_{GT(-)}$ denotes the gap between two major GT(−) energies. The experimental $M1$ energy, 10.23 MeV [79], is indicated by a dashed line. The experimental low-lying and giant GT(−) energies, 2.517 MeV [75] and 10.8 MeV [80], respectively, are indicated by solid lines.

$M1$-strength height B_{M1} decreases when the IV-PV coupling becomes stronger [3], whereas in contrast the higher-energy GT(−) strength B_{GT} increases [15]. This opposite behavior can be attributed to the fact that the IV-PV residual interaction in the nonrelativistic limit yields the spin-isospin form of $(\vec{s}_1 \cdot \vec{s}_2)(\vec{t}_1 \cdot \vec{t}_2)$ [12,15], and thus enhances the isospin-singlet, $\nu(1f_{7/2}) \longrightarrow \pi(1f_{5/2})$ component in the GT(−) case. In parallel, the $\nu(1f_{7/2}) \longrightarrow \nu(1f_{5/2})$ component in the $M1$ excitation is suppressed because the PV interaction does not support this isospin-triplet component. Notice also that the low-lying GT(−) strength is suppressed; namely, the PV interaction does not promote the $\nu(1f_{7/2}) \longrightarrow \pi(1f_{7/2})$ component. A similar change of GT strength with the residual interaction was reported in Refs. [15,89].

Figure 3 displays the $M1$ and GT excitation energies for ^{48}Ca, calculated with the RRPA using DD-PC1 and DD-PCX interactions, and the IV-PV residual interaction for the range of values of its strength parameter $\alpha_{IV-PV} = 0$–2.1 fm^2. If the simple shell-model picture is a good approximation, the $M1$ excitation energy, E_{M1}, is consistent to the SO splitting of neutron levels [37,38], whereas the gap of giant and low-lying GT energies, $\Delta E_{GT(-)}$, corresponds to the proton SO splitting [27,54]. As confirmed in the previous nonperturbed results with $\alpha_{IV-PV} = 0$, the E_{M1} and $\Delta E_{GT(-)}$ values coincide except for a small gap due to the Coulomb-repulsion potential on the proton side. We checked that these values are indeed equivalent to the SO-splitting gaps of neutrons and protons in the numerical ground-state solutions. Then, by increasing the α_{IV-PV} value, the difference of E_{M1} and $\Delta E_{GT(-)}$ values becomes wider. This tendency is confirmed both in the DD-PC1 and DD-PCX cases. Consequently, the IV-PV residual interaction affects both $M1$ and GT energies but in different ways. This inequality is attributed to the spin-isospin character
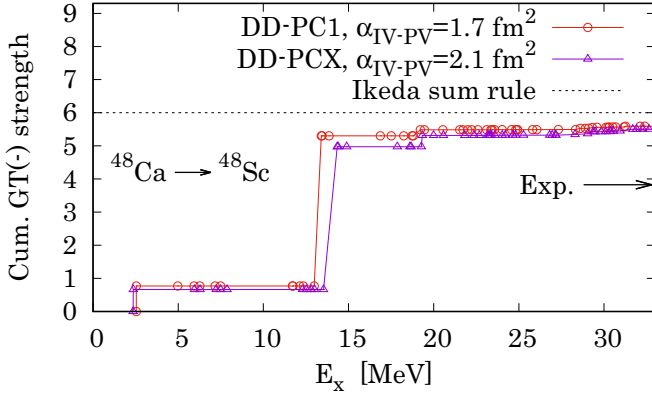
FIG. 4. Cumulative GT$(-)$ strength for ^{48}Ca obtained from our RRPA method. The Ikeda-Fujii-Fujita sum rule as in Eq. (14) is plotted by the dotted line. The arrow indicates the experimental value of $\sum B_{\text{GT}(-)} = 15.3/4$ up to 30 MeV [80].

of the IV-PV interaction, whose effect is not common between the neutron-neutron (NN) and PN configurations in the $M1$ and GT transitions, respectively.

In Fig. 4, the cumulative GT$(-)$ strength for ^{48}Ca is plotted. This is defined as [19,31]

$$S_{\text{GT}(-)}(E_{\text{x}}) = \int_0^{E_{\text{x}}} dE \frac{dB_{\text{GT}(-)}(E)}{dE}$$
$$= \int_0^{E_{\text{x}}} dE R_{\text{GT}(-)}(E), \qquad (13)$$

where $R_{\text{GT}(-)}(E)$ is the response function in Eq. (12). Also, for comparison, it is convenient to use the Ikeda-Fujii-Fujita sum rule [32,33]. That is,

$$\lim_{E_{\text{x}} \to \infty} [S_{\text{GT}(-)}(E_{\text{x}}) - S_{\text{GT}(+)}(E_{\text{x}})] = \frac{3(N-Z)}{4}, \qquad (14)$$

from the total GT$(\pm)$ summations. Notice the factor $1/4$ because we use the spin operator $\hat{s}$ instead of $\hat{\sigma} = 2\hat{s}$. For the Ca nuclei, the GT$(+)$ response is strongly suppressed due to the Pauli blocking effect, namely, $S_{\text{GT}(+)}(E_{\text{x}} \to \infty) \cong 0$. In Fig. 4, our cumulative GT strength is consistent with the Ikeda-Fujii-Fujita sum rule, $S_{\text{GT}(-)}(E_{\text{x}} \to \infty) \cong 6$ for ^{48}Ca, with a small deficiency of $\cong 8\%$ due to omitting the Dirac-sea states [14]. There are two main jumps at $E_{\text{x}} \cong 2.5$ MeV and $E_{\text{x}} \cong 13$ MeV in correspondence with the GT excitation energies in Fig. 2. Note that the similar result is obtained from the nonrelativistic RPA [31]. However, the experimental data yield $\sum B_{\text{GT}(-)} = 15.3 \pm 2.2$ up to 30 MeV [80], which is lower than our result, $4S_{\text{GT}(-)}(E_{\text{x}} \leqslant 30 \text{ MeV}) \cong 22$. This discrepancy is due to the missing high-energy GT strength in experiments, and thus, the Ikeda-Fujii-Fujita sum rule is not shown as applicable. Indeed in Ref. [31], by employing the subtracted second RPA, the GT strength is shown to be more fragmented and in better agreement with experimental data [80]. The similar method in the REDF framework, however, is technically challenging, and beyond the present study.
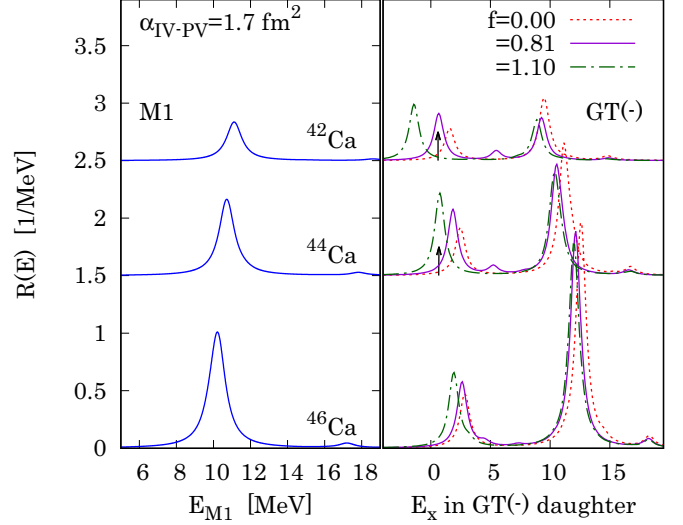

FIG. 5. The IV-spin-$M1$ and GT$(-)$ strength distributions for $^{42-46}$Ca nuclei with the DD-PC1 and the IV-PV interaction with $\alpha_{\text{IV-PV}} = 1.7$ fm^2. The GT$(-)$ response is shown for three values of PN pairing strength, $f = 0, 0.81$, and 1.1. Vertical arrows indicate the low-lying GT$(-)$ energies in experiment [55,75]: for ^{42}Ca $\longrightarrow$ ^{42}Sc, 0.611 MeV; for ^{44}Ca $\longrightarrow$ ^{44}Sc, 0.667 MeV.

C. Open-shell Ca isotopes

In the following sections, except when modified, we commonly use the DD-PC1 plus IV-PV Lagrangian with $\alpha_{\text{IV-PV}} = 1.70$ fm^2 adjusted to the experimental $M1$ and GT energies of ^{48}Ca. For open-shell nuclei, the pairing correlations should be taken into account. As explained in Sec. II, the T1 pairing is described by the pairing part of the Gogny-D1S force as used in Refs. [11,68]. The PN (T0) pairing is described by the two-Gaussian potential as given in Refs. [73,74].

Figure 5 shows our results for $^{42-46}$Ca. In Fig. 5, the GT$(-)$ response is shown for three values of PN pairing strength, $f = 0.0, 0.81$, and 1.1 in Eq. (4). This PN pairing indeed plays an essential role to reproduce the low-lying GT energy, which appears higher than the experimental data when the PN pairing is neglected. For instance, the PN pairing with $f = 0.81$ reproduces the low-lying GT$(-)$ excitation of ^{42}Sc at 0.611 MeV [55,75]. Note that the similar GT distribution and the decrease of GT$(-)$ energy by the PN-pairing interaction were predicted from the Skyrme QRPA [19]. For ^{44}Ca, however, there still remains a finite gap between the calculated and experimental low-lying GT energies: the enhancement of $f = 1.1$ is instead necessary for this system. It suggests that, instead of the PN pairing strength commonly used for all the isotopes, one needs the system-dependent fine-tuning of PN pairing strength and/or further complicated model for quantitative agreement. This observation agrees with applications of the RQRPA in the calculation of β-decay half-lives, where it was found that a single value of PN pairing strength cannot reproduce experimental half-lives across the isotopic chain [23,24,90,91].

In Fig. 5, the absolute strengths of the $M1$ and giant-GT transitions from ^{42}Ca become comparable by using the
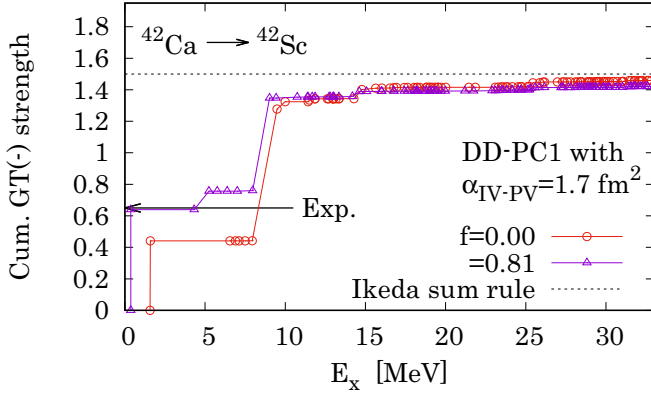
FIG. 6. Cumulative GT($-$) strength for ^{42}Ca obtained with the DD-PC1 plus IV-PV interaction with $\alpha_{\text{IV-PV}} = 1.7$ fm^2. The Ikeda-Fujii-Fujita sum rule as in Eq. (14) is plotted by the dotted line. The arrow indicates the experimental value of $\sum B_{\text{GT}(-)} = 2.6/4$ [55].

PN pairing interaction with $f = 0.81$: $R_{\text{M1}} = 0.34$ MeV^{-1} at $E_{\text{M1}} = 11.1$ MeV in ^{42}Ca, whereas $R_{\text{GT}(-)} = 0.37$ MeV^{-1} at $E_{\text{x}} = 9.3$ MeV in the GT($-$) daughter ^{42}Sc nucleus. Namely, the $M1$-GT equivalence, which was disrupted by the IV-PV interaction for closed-shell nuclei in Fig. 2, is in this case restored. However, that restoring effect is less visible in the neutron-rich Ca nuclei. In the ^{44}Ca case, for instance, a stronger attractive PN pairing with $f = 1.1$ is necessary to reproduce its experimental low-lying GT energy. However, there is still a finite difference between its $M1$ and giant-GT strengths: $R_{\text{M1}} = 0.66$ MeV^{-1} at $E_{\text{M1}} = 10.72$ MeV in ^{44}Ca, whereas $R_{\text{GT}(-)} = 0.91$ MeV^{-1} at $E_{\text{x}} = 10.35$ MeV in ^{44}Sc in Fig. 5.

Notice that, by using $f = 1.1$, the low-lying GT($-$) response in ^{42}Sc shows the negative excitation energy. Namely, this GT($-$) state results lower than the experimental ground state, because of the overenhancement of the PN-pairing attractive interaction.

In Fig. 6, the cumulative GT($-$) strength for ^{42}Ca is plotted. Our cumulative GT strength is consistent with the Ikeda-Fujii-Fujita sum rule, $S_{\text{GT}(-)}(E_{\text{x}} \to \infty) \cong 1.5$ for ^{42}Ca, whereas the GT($+$) response is negligible due to the Pauli blocking effect. With $f = 0.81$ for the PN pairing, there are two main jumps at $E_{\text{x}} \cong 0.6$ and $\cong 9$ MeV in correspondence with the two major peaks shown in Fig. 5. However, in recent experimental data [55], the second jump has not been confirmed. In Ref. [55], the measured value of total GT strength for ^{42}Ca $\longrightarrow$ ^{42}Sc is $2.6/4 = 0.65$, where the factor $1/4$ is needed for the present comparison. This value is close to our result, 0.64 with $f = 0.81$ but only from the first peak at $E_{\text{x}} = 0.6$ MeV in Fig. 6. Namely, the RQRPA calculation can be valid but mainly in the low-lying region. One possible reason for the absence of experimental GT($-$) strength especially in the high-energy region is the continuum coupling, where the GT($-$) excitation brings the final-state proton above the one-proton threshold, and thus, its width can be large. Another possibility is the effect of higher-order configurations beyond the present RQRPA level, as we mentioned in the ^{48}Ca case [31].
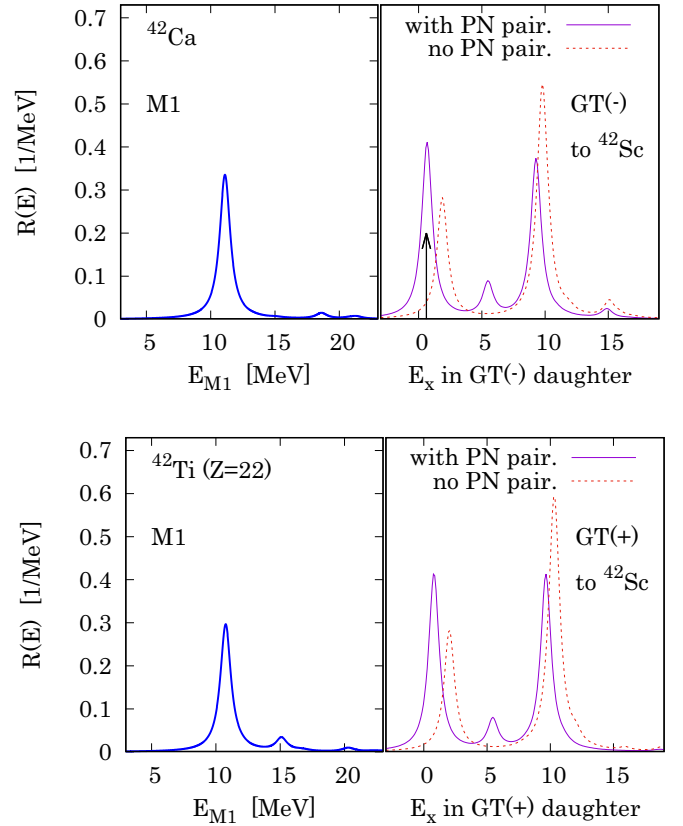

FIG. 7. The IV-spin-$M1$ and GT strength distributions of ^{42}Ca and ^{42}Ti obtained with the DD-PC1 plus IV-PV interaction with $\alpha_{\text{IV-PV}} = 1.7$ fm^2. For GT($\pm$) modes, their excitation energies are presented with respect to the common daughter nucleus ^{42}Sc. The arrow indicates the experimental low-lying GT($-$) energy 0.611 MeV in ^{42}Sc [75].

Before closing our discussion, we check the mirror symmetry in terms of the $M1$ and GT transitions. For this purpose, calculations are performed for ^{42}Ti, which is the mirror system of ^{42}Ca. Figure 7 shows our results. The GT($+$) strength function from ^{42}Ti coincides well with the GT($-$) strength function from ^{42}Ca, where their daughter nucleus is common, ^{42}Sc. In particular, the RQRPA predicts the low-lying GT($+$) state equivalently to the GT($-$) case. The PN pairing is again found as essential to reproduce its energy. For the $M1$ transition, these two isobaric-analog nuclei have consistent $M1$ excitation energy and strength. This can be naturally understood from that their $M1$ transitions are mainly attributed to the $f_{7/2} \longrightarrow f_{5/2}$ transition in the proton (neutron) side for ^{42}Ti (^{42}Ca). Consequently, the mirror symmetry holds both in the $M1$ and GT($\pm$) transitions. However, we note that the $M1$ excitation energy in ^{42}Ti predicted here is much higher than the one-proton-separation threshold, 3.75 MeV [84], and thus its fragmentation can be wider than the width used in smearing our RQRPA spectra. Measurement of this continuum $M1$ state is thus expected to be challenging.

IV. SUMMARY

We discussed the isobaric-analog symmetry between the $M1$ and GT transitions in Ca isotopes by investigating their

excitation energies and transition strengths. The symmetry of unperturbed $M1$ and GT response can be broken by including the IV-PV residual interaction in the R(Q)RPA, which affects the $M1$ and GT strengths inequivalently. This is explained by the spin-isospin character of the interaction, whose effect is not common for the NN and PN configurations in the $M1$ and GT transitions, respectively. The isoscalar PN pairing effect is also considered for open-shell nuclei. This effect is found indispensable to reproduce their low-lying GT energies [19,90,91]. Due to the interplay between the IV-PV and pairing channels in the RQRPA, the GT-$M1$ symmetry can be restored in the open-shell ^{42}Ca nucleus; i.e., the giant GT excitation shows its strength being comparable to that of the $M1$ excitation. A remarkable agreement between the GT($\pm$) transitions is predicted for ^{42}Ca and ^{42}Ti nuclei, implying the mirror symmetry. This mirror symmetry is predicted also in their $M1$ transitions.

The validity of IV-PV parametrization is also discussed with respect to the experimental $M1$ and GT excitation energies. We conclude that, within the present DD-PC1 (DD-PCX) plus IV-PV parametrization, the accurate and simultaneous reproduction of $M1$ and GT transition energies for various nuclei is still rather challenging. This problem suggests that further improvements of the REDF, especially for the SO splittings, are required, as well as more advanced formulation of the PV coupling.

The quenching effect is not considered in this work. Whether the common quenching can be valid or not for IV-$M1$ and GT modes is an open and essential problem, to which we are aiming to approach. A similar question has been discussed between the IS and IV modes of $M1$ [47], which the RQRPA could answer in the near future. We note that it could also be interesting to discuss the GT/$M1$ properties in deformed nuclei. However, this task requires a development of the deformed relativistic QRPA and intensive computations. We aim to address this topic in our future work.
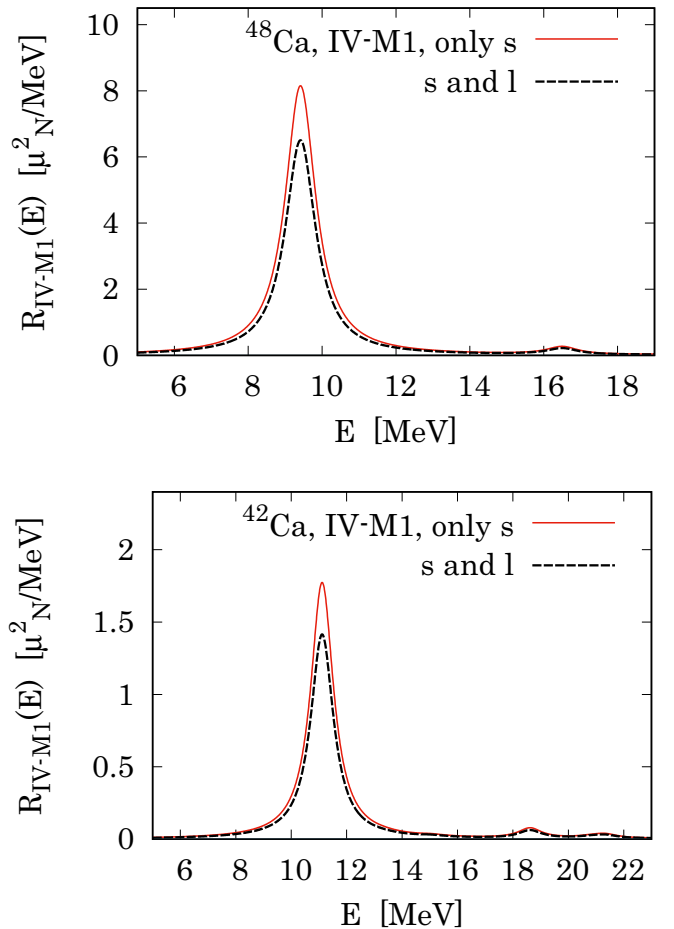
FIG. 8. The IV-$M1$ response functions for ^{42,48}Ca nuclei.

APPENDIX: INCLUSION OF ORBITAL $M1$ COMPONENT

In this section, we investigate the effect of the orbital-$M1$ component. The original IV-$M1$ operator is given in Eq. (6) in the main text, including both $\hat{\tau}_0\hat{s}_\nu$ and $\hat{\tau}_0\hat{l}_\nu$ terms. We perform the RQRPA calculations by using these operators. Note that the factor $\mu_N\sqrt{3/4\pi}$ and g factors, $g_s = 4.706$ and $g_l = 1/2$, are taken into account in this section. The DD-PC1 and T1 pairing interactions are utilized similarly to the main text. The IV-PV coupling of $\alpha_{\text{IV-PV}} = 1.7$ fm^2 is also used in the R(Q)RPA-residual interactions.

In Fig. 8, our results for the ^{48}Ca and ^{42}Ca nuclei are displayed. There we compare the two cases, where the orbital-$M1$ operator, $g_l\mu_N\sqrt{3/4\pi} \cdot \hat{\tau}_0\hat{l}_\nu$ is neglected (only s) or included (s and l). It is shown that the inclusion of the orbital-$M1$ component reduces the IV-$M1$ strength of these nuclei. We checked that, in terms of $M1$-response summation, which reads $\int R_{M1}(E)dE$, this reduction is approximately 80% of the "only s" case. Since the orbit-$M1$ inclusion is shown as another source of quenching of B_{M1}, a careful treatment is necessary in forthcoming studies. However, the major excitation energies are not affected even if the orbital-$M1$ component is included. This is natural because the selection rule of spin and orbital IV-$M1$ operators are identical [25]. Therefore, the active excited states in the R(Q)RPA calculations should be common and have the same eigenenergies.

[1] H. Ejiri, P. Richard, S. Ferguson, R. Heffner, and D. Perry, Phys. Rev. Lett. **21**, 373 (1968).

[2] H. Ejiri, A. I. Titov, M. Boswell, and A. Young, Phys. Rev. C **88**, 054610 (2013).

[3] E. Migli, S. Drozdz, J. Speth, and J. Wambach, Z. Phys. A **340**, 111 (1991).

[4] S. P. Kamerdzhiev and V. N. Tkachev, Z. Phys. A Atomic Nucl. **334**, 19 (1989).

[5] F. Grümmer and J. Speth, J. Phys. G: Nucl. Part. Phys. **32**, R193 (2006).

[6] P. Vesely, J. Kvasil, V. O. Nesterenko, W. Kleinig, P. G. Reinhard, and V. Y. Ponomarev, Phys. Rev. C **80**, 031302(R) (2009).

[7] V. O. Nesterenko, J. Kvasil, P. Vesely, W. Kleinig, P.-G. Reinhard, and V. Y. Ponomarev, J. Phys. G: Nucl. Part. Phys. **37**, 064034 (2010).

[8] V. O. Nesterenko, J. Kvasil, P. Vesely, W. Kleinig, and P.-G. Reinhard, Int. J. Mod. Phys. E **19**, 558 (2010).

[9] V. Tselyaev, N. Lyutorovich, J. Speth, P.-G. Reinhard, and D. Smirnov, Phys. Rev. C **99**, 064329 (2019).

[10] J. Speth, P.-G. Reinhard, V. Tselyaev, and N. Lyutorovich, arXiv:2001.07236.

[11] G. Kružić, T. Oishi, D. Vale, and N. Paar, Phys. Rev. C **102**, 044315 (2020).

[12] T. Oishi, G. Kružić, and N. Paar, J. Phys. G: Nucl. Part. Phys. **47**, 115106 (2020).

[13] D. Vretenar, N. Paar, T. Nikšić, and P. Ring, Phys. Rev. Lett. **91**, 262502 (2003).

[14] N. Paar, T. Nikšić, D. Vretenar, and P. Ring, Phys. Rev. C **69**, 054303 (2004).

[15] Z.-Y. Ma, C. B.-Q., N. Van Giai, and T. Suzuki, Eur. Phys. J. A **20**, 429 (2004).

[16] Y. F. Niu, G. Colò, M. Brenna, P. F. Bortignon, and J. Meng, Phys. Rev. C **85**, 034314 (2012).

[17] X. Roca-Maza, G. Colò, and H. Sagawa, Phys. Rev. C **86**, 031306(R) (2012).

[18] K. Yoshida, Prog. Theor. Exp. Phys. **2013**, 113D02 (2013).

[19] C. L. Bai, H. Sagawa, G. Colò, Y. Fujita, H. Q. Zhang, X. Z. Zhang, and F. R. Xu, Phys. Rev. C **90**, 054335 (2014).

[20] T. Oishi and N. Paar, Phys. Rev. C **100**, 024308 (2019).

[21] F. Minato and Y. Tanimura, Eur. Phys. J. A **56**, 45 (2020).

[22] D. Vale, Y. F. Niu, and N. Paar, Phys. Rev. C **103**, 064307 (2021).

[23] A. Ravlić, Y. F. Niu, T. Nikšić, N. Paar, and P. Ring, Phys. Rev. C **104**, 064302 (2021).

[24] A. Ravlić, E. Yüksel, Y. F. Niu, and N. Paar, Phys. Rev. C **104**, 054318 (2021).

[25] J. Suhonen, *From Nucleons to Nucleus: Concepts of Microscopic Nuclear Theory* (Springer-Verlag, Berlin, 2007).

[26] F. Osterfeld, Rev. Mod. Phys. **64**, 491 (1992).

[27] Y. Fujita, B. Rubio, and W. Gelletly, Prog. Part. Nucl. Phys. **66**, 549 (2011).

[28] T. Kajino, W. Aoki, A. Balantekin, R. Diehl, M. Famiano, and G. Mathews, Prog. Part. Nucl. Phys. **107**, 109 (2019).

[29] H.-T. Janka, K. Langanke, A. Marek, G. Martínez-Pinedo, and B. Müller, Phys. Rep. **442**, 38 (2007), the Hans Bethe Centennial Volume 1906-2006.

[30] K. Langanke, G. Martínez-Pinedo, and R. G. T. Zegers, Rep. Prog. Phys. **84**, 066301 (2021).

[31] D. Gambacurta, M. Grasso, and J. Engel, Phys. Rev. Lett. **125**, 212501 (2020).

[32] K. Ikeda, S. Fujii, and J. I. Fujita, Phys. Lett. **3**, 271 (1963).

[33] J. I. Fujita, S. Fujii, and K. Ikeda, Phys. Rev. **133**, B549 (1964).

[34] G. F. Bertsch and I. Hamamoto, Phys. Rev. C **26**, 1323 (1982).

[35] M. Bender, J. Dobaczewski, J. Engel, and W. Nazarewicz, Phys. Rev. C **65**, 054322 (2002).

[36] N. Paar, D. Vretenar, E. Khan, and G. Coló, Rep. Prog. Phys. **70**, R02 (2007).

[37] K. Heyde, P. von Neumann-Cosel, and A. Richter, Rev. Mod. Phys. **82**, 2365 (2010), and references therein.

[38] N. Pietralla, P. von Brentano, and A. Lisetskiy, Prog. Part. Nucl. Phys. **60**, 225 (2008).

[39] A. Richter, Prog. Part. Nucl. Phys. **13**, 1 (1985).

[40] A. Richter, Nucl. Phys. A **507**, 99 (1990).

[41] T. Shizuma, T. Hayakawa, H. Ohgaki, H. Toyokawa, T. Komatsubara, N. Kikuzawa, A. Tamii, and H. Nakada, Phys. Rev. C **78**, 061303(R) (2008).

[42] L.-G. Cao, G. Colò, H. Sagawa, P. F. Bortignon, and L. Sciacchitano, Phys. Rev. C **80**, 064304 (2009).

[43] S. Goriely, S. Hilaire, S. Péru, M. Martini, I. Deloncle, and F. Lechaftois, Phys. Rev. C **94**, 044306 (2016).

[44] T. Otsuka, T. Suzuki, R. Fujimoto, H. Grawe, and Y. Akaishi, Phys. Rev. Lett. **95**, 232502 (2005).

[45] K. Langanke, G. Martínez-Pinedo, P. von Neumann-Cosel, and A. Richter, Phys. Rev. Lett. **93**, 202501 (2004), and references therein.

[46] H. P. Loens, K. Langanke, G. Martinez-Pinedo, and K. Sieja, Eur. Phys. J. A **48**, 34 (2012).

[47] H. Matsubara, A. Tamii, H. Nakada, T. Adachi, J. Carter, M. Dozono, H. Fujita, K. Fujita, Y. Fujita, K. Hatanaka, W. Horiuchi, M. Itoh, T. Kawabata, S. Kuroita, Y. Maeda, P. Navrátil, P. von Neumann-Cosel, R. Neveling, H. Okamura, L. Popescu *et al.*, Phys. Rev. Lett. **115**, 102501 (2015).

[48] S. Goriely, E. Khan, and M. Samyn, Nucl. Phys. A **739**, 331 (2004).

[49] S. Goriely, A. Bauswein, and H.-T. Janka, Astrophys. J. **738**, L32 (2011).

[50] D. Kurath, Phys. Rev. **130**, 1525 (1963).

[51] B. D. Anderson, T. Chittrakarn, A. R. Baldwin, C. Lebo, R. Madey, P. C. Tandy, J. W. Watson, B. A. Brown, and C. C. Foster, Phys. Rev. C **31**, 1161 (1985).

[52] T. Wakasa, H. Sakai, H. Okamura, H. Otsu, S. Fujita, S. Ishida, N. Sakamoto, T. Uesaka, Y. Satou, M. B. Greenfield, and K. Hatanaka, Phys. Rev. C **55**, 2909 (1997).

[53] M. Ichimura, H. Sakai, and T. Wakasa, Prog. Part. Nucl. Phys. **56**, 446 (2006).

[54] Y. Fujita, B. Rubio, T. Adachi, F. Molina, A. Algora, G. P. A. Berg, P. von Brentano, J. Buscher, T. Cocolios, D. D. Frenne, C. Fransen, H. Fujita, K. Fujita, W. Gelletly, K. Hatanaka, M. Huyse, O. Ivanov, Y. Kudryavtsev, E. Jacobs, D. Jordán *et al.*, J. Phys. G: Nucl. Part. Phys. **35**, 014041 (2008).

[55] Y. Fujita, H. Fujita, T. Adachi, C. L. Bai, A. Algora, G. P. A. Berg, P. von Brentano, G. Colò, M. Csatlós, J. M. Deaven, E. Estevez-Aguado, C. Fransen, D. De Frenne, K. Fujita, E. Ganioğlu, C. J. Guess, J. Gulyás, K. Hatanaka, K. Hirota, M. Honma *et al.*, Phys. Rev. Lett. **112**, 112502 (2014).

[56] G. M. Crawley, C. Djalali, N. Marty, M. Morlet, A. Willis, N. Anantaraman, B. A. Brown, and A. Galonsky, Phys. Rev. C **39**, 311 (1989).

[57] J. Birkhan, H. Matsubara, P. von Neumann-Cosel, N. Pietralla, V. Y. Ponomarev, A. Richter, A. Tamii, and J. Wambach, Phys. Rev. C **93**, 041302(R) (2016).

[58] P. von Neumann-Cosel and A. Tamii, Eur. Phys. J. A **55**, 110 (2019).

[59] J. D. Walecka, Ann. Phys. **83**, 491 (1974).

[60] J. Boguta and A. Bodmer, Nucl. Phys. A **292**, 413 (1977).

[61] P.-G. Reinhard, Rep. Prog. Phys. **52**, 439 (1989).

[62] D. Vretenar, A. V. Afanasjev, G. A. Lalazissis, and P. Ring, Phys. Rep. **409**, 101 (2005), and references therein.

[63] J. Meng, H. Toki, S. Zhou, S. Zhang, W. Long, and L. Geng, Prog. Part. Nucl. Phys. **57**, 470 (2006).

[64] T. Nikšić, D. Vretenar, and P. Ring, Prog. Part. Nucl. Phys. **66**, 519 (2011).

[65] J.-P. Ebran, A. Mutschler, E. Khan, and D. Vretenar, Phys. Rev. C **94**, 024304 (2016).

[66] N. Paar, P. Ring, T. Nikšić, and D. Vretenar, Phys. Rev. C **67**, 034312 (2003).

[67] T. Nikšić, T. Marketin, D. Vretenar, N. Paar, and P. Ring, Phys. Rev. C **71**, 014308 (2005).

[68] T. Nikšić, N. Paar, D. Vretenar, and P. Ring, Comput. Phys. Commun. **185**, 1808 (2014).

[69] T. Nikšić, D. Vretenar, and P. Ring, Phys. Rev. C **78**, 034318 (2008).

[70] E. Yüksel, T. Marketin, and N. Paar, Phys. Rev. C **99**, 034318 (2019).

[71] B. Podobnik, D. Vretenar, and P. Ring, Z. Phys. A **354**, 375 (1996).

[72] J. F. Berger, M. Girod, and D. Gogny, Comput. Phys. Commun. **63**, 365 (1991).

[73] E. Yüksel, N. Paar, G. Colò, E. Khan, and Y. F. Niu, Phys. Rev. C **101**, 044305 (2020).

[74] A. Ravlić, E. Yüksel, Y. F. Niu, G. Colò, E. Khan, and N. Paar, Phys. Rev. C **102**, 065804 (2020).

[75] Y. Fujita, Y. Utsuno, and H. Fujita, Eur. Phys. J. A **56**, 138 (2020).

[76] J. Eisenber and W. Greiner, *Nuclear Theory Volume 2: Excitation Mechanisms of the Nucleus* (North-Holland, Amsterdam, 1970).

[77] Y. Fujita, H. Akimune, I. Daito, M. Fujiwara, M. N. Harakeh, T. Inomata, J. Jänecke, K. Katori, C. Lüttge, S. Nakayama, P. von Neumann-Cosel, A. Richter, A. Tamii, M. Tanaka, H. Toyokawa, H. Ueno, and M. Yosoi, Phys. Rev. C **55**, 1137 (1997).

[78] P. Ring and P. Schuck, *The Nuclear Many-Body Problems* (Springer-Verlag, Berlin, 1980).

[79] J. R. Tompkins, C. W. Arnold, H. J. Karwowski, G. C. Rich, L. G. Sobotka, and C. R. Howell, Phys. Rev. C **84**, 044331 (2011).

[80] K. Yako, M. Sasano, K. Miki, H. Sakai, M. Dozono, D. Frekers, M. B. Greenfield, K. Hatanaka, E. Ihara, M. Kato, T. Kawabata, H. Kuboki, Y. Maeda, H. Matsubara, K. Muto, S. Noji, H. Okamura, T. H. Okabe, S. Sakaguchi, Y. Sakemi *et al.*, Phys. Rev. Lett. **103**, 012503 (2009).

[81] R. M. Laszewski, R. Alarcon, D. S. Dale, and S. D. Hoblit, Phys. Rev. Lett. **61**, 1710 (1988).

[82] H. Akimune, I. Daito, Y. Fujita, M. Fujiwara, M. Greenfield, M. Harakeh, T. Inomata, J. Jänecke, K. Katori, S. Nakayama, H. Sakai, Y. Sakemi, M. Tanaka, and M. Yosoi, Phys. Lett. B **323**, 107 (1994).

[83] T. Wakasa, M. Okamoto, M. Dozono, K. Hatanaka, M. Ichimura, S. Kuroita, Y. Maeda, H. Miyasako, T. Noro, T. Saito, Y. Sakemi, T. Yabe, and K. Yako, Phys. Rev. C **85**, 064606 (2012).

[84] Chart of Nuclides, National Nuclear Data Center (NNDC), http://www.nndc.bnl.gov/chart/.

[85] K. Mizuyama, M. Matsuo, and Y. Serizawa, Phys. Rev. C **79**, 024313 (2009).

[86] K. Mizuyama, G. Colò, and E. Vigezzi, Phys. Rev. C **86**, 034318 (2012).

[87] L. E. Marcucci, M. Pervin, S. C. Pieper, R. Schiavilla, and R. B. Wiringa, Phys. Rev. C **78**, 065501 (2008).

[88] S. Moraghe, J. Amaro, C. García-Recio, and A. Lallena, Nucl. Phys. A **576**, 553 (1994).

[89] C. L. Bai, H. Q. Zhang, X. Z. Zhang, F. R. Xu, H. Sagawa, and G. Colò, Phys. Rev. C **79**, 041301(R) (2009).

[90] Z. Niu, Y. Niu, H. Liang, W. Long, T. Nikšić, D. Vretenar, and J. Meng, Phys. Lett. B **723**, 172 (2013).

[91] T. Marketin, L. Huther, and G. Martínez-Pinedo, Phys. Rev. C **93**, 025805 (2016).